COMMUNICATION

Check for updates

Optically-regulated thermal energy storage in diverse organic phase-change materials†

Grace G. D. Han, [ID] [a] Joshua H. Deru, [b] Eugene N. Cho [ID] [a] and Jeffrey C. Grossman [ID] *[a]

Thermal energy storage and release in aliphatic phase-change materials are actively controlled by adding azobenzene-based photo-switches. UV activation of the additives induces supercooling of the composites, allowing for longer thermal storage at lower temperatures. The mechanism of this process is studied by comparing phase change behavior across diverse materials.

Low-grade thermal energy storage in organic phase-change materials (PCMs) *via* solid–liquid phase transition shows potential efficacy in unique applications including thermo-regulating fabrics,[1] temperature-adaptable buildings,[2] and thermal protection of electronic devices,[3] biomedical products,[4] and food[5] due to the low melting points (between 0 and 250 °C),[6] low cost,[7] and diverse form factors[8,9] that organic PCMs present. Latent heat storage provides generally higher storage capacity and efficiency than sensible heat storage and also enables heat release at a targeted temperature determined by the phase transition temperature.[10] One drawback of latent heat storage in PCM is the sole dependence of PCM crystallization on the ambient temperature and consequent lack of control in determining when the stored energy is released.[11] Nano-confinement of organic PCMs in diverse porous materials,[12] particularly carbon-based materials such as carbon aerogels[13] and graphene oxides,[14] has been reported as a successful method which increases thermal conductivity of PCM composites and shifts crystallization points (T_C) of PCMs. However, the nano-confined PCMs still exhibit fixed T_C, determined by the composition of PCMs and nano-structured host materials, thus their phase passively responds to the changing ambient temperature.

Recently, we developed an active and dynamic method to prevent crystallization as the PCM cools to temperatures below

the original phase transition temperature by incorporating photo-switching dopants.[15] Although photo-switches were previously investigated as dopants in liquid crystals[16–18] to optically change their phases, the application in thermal energy storage as integrated to traditional latent heat storage materials was newly discovered. In that proof-of-concept work, we demonstrated that the liquid phase of an organic PCM, tridecanoic acid, can be preserved at temperatures lower than its pure-phase crystallization point due to the increased interaction with photo-switching azobenzene dopants upon UV activation. When cooled below T_C the new energy barrier for the liquid-to-solid transition introduced by the presence of switched azobenzene dopants[19] can be overcome by simple visible light illumination, which switches the dopants back to their starting configuration and triggers the heat release from the liquid PCM composite. This hybrid photo-switch/PCM system demonstrated prolonged thermal storage well below the original T_C, enabled by the activated photo-switches, without compromising storage capacity due to the presence of metastable *cis* dopants that store additional thermal energy.[15] The hybrid system show stability over 100 cycles (50 hours of fast cycling operation) and thermal storage time over 10 hours under a supercooled condition, while pristine PCMs crystallize within minutes when cooled below T_C.

Herein, we explore the optical regulation of thermal energy storage in diverse aliphatic PCMs and demonstrate the different degrees of lowering T_C of each PCM depending on their chain lengths and functional groups. The structures of the PCMs determine the degree of intermolecular interaction and the operation temperature of heat storage, and our results shed light on parameters and conditions that can be controlled to change the nucleation and crystallization of this class of thermal storage materials.

The strategy to make the T_C of organic PCMs optically triggerable is described in Fig. 1a. Upon heat absorption, the PCMs first melt (T_m ranging from 10 to 70 °C) while the azobenzene dopants with higher melting point of 73 °C remain aggregated and dispersed in the liquid PCM. UV illumination on the suspension activates *trans*-Azo dopants to isomerize into
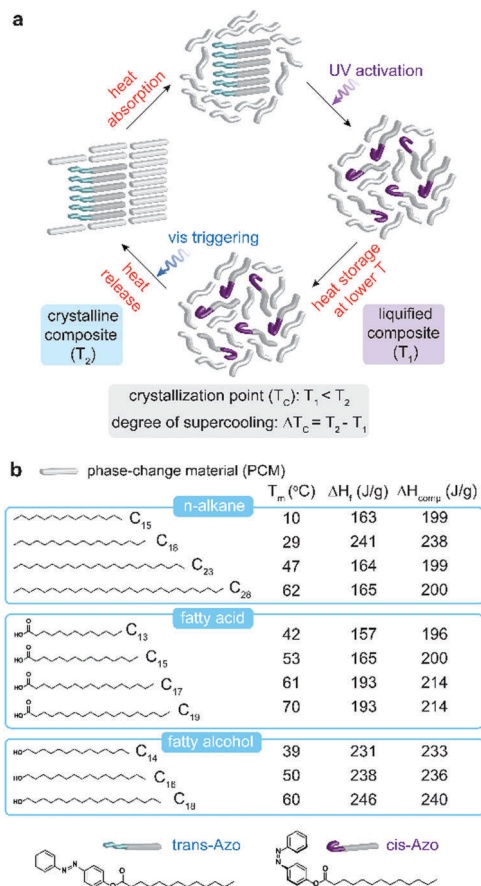
[a] *Department of Materials Science and Engineering, Massachusetts Institute of Technology, 77 Massachusetts Avenue, Cambridge, MA, 02139, USA. E-mail: jcg@mit.edu*

[b] *Department of Materials, University of Oxford, 16 Parks Road, Oxford, OX1 3PH, UK*

Fig. 1 (a) Schematic illustration of heat storage and release cycle in the composite of PCMs and photo-switching dopants. (b) Chemical structures of PCMs investigated in this work along with their melting point (T_m), their intrinsic heat of fusion (ΔH_f), and heat storage capacity of respective composites containing 50 wt% azobenzene dopants (ΔH_{comp}). We note that the ΔH_{comp} values are estimated, based on the calculations (Supporting Note 1, ESI†). Chemical structures of photo-switching dopants in two isomeric conformations before and after UV activation.

the *cis*, which presents higher polarity and steric bulk compared to the *trans* form. The interaction between *cis*-Azo and the liquid PCM molecules effectively stabilizes the liquid phase of the composite down to lower temperatures than the intrinsic T_C of the initial composite (T_2) with *trans*-Azo. The new T_C of the UV-activated composite (T_1) and the difference between T_1 and T_2, defined as ΔT_C, become important metrics for the system. ΔT_C, in particular, represents the degree of light-induced supercooling obtained in each composite or the range of temperature over which the liquid-phase heat storage material is stabilized without losing heat through solidification. The stored heat can be released by optical triggering with visible light which causes the *cis*-to-*trans* reverse isomerization, aggregation of *trans*-Azo which forms nucleation seeds, and the rapid crystallization of the PCM composite.

The structural variation of aliphatic organic PCMs (Fig. 1b) provides a wide range of melting points (T_m), which defines temperatures of heat storage, and heat of fusion (ΔH_f) that generally increases as the chain becomes longer, despite some exceptions.[20]

Three groups of aliphatic PCMs including *n*-alkane,[21] fatty acid,[22] and fatty alcohol,[23] were investigated in this study to expand the scope of PCMs and to compare the impact of relative polarity of PCMs on the efficiency of heat storage and on the intermolecular interactions that operate the heat storage cycle. We used one type of azobenzene dopant with a C_{13} chain, unlike the previous work[15] that investigated the variation of dopant structures, in order to now focus on the role of PCM types and their interaction with the azobenzene unit upon isomerization. The expected heat storage capacities in the composites are listed next to the heat of fusion of pristine PCMs based on assuming complete *cis*-to-*trans* conversion of dopants and complete crystallization of composites (Supporting Note 1, ESI†).

With the aim of maximizing the degree of supercooling (ΔT_C), we first varied the ratio of dopants in the PCMs (Fig. 2a) which resulted in volcano-shaped plots (ΔT_C *vs.* additive ratio) for two distinct PCMs with significantly different polarity, chain length, and melting point. Highly polar C_{13}-acid exhibits a max. ΔT_C of 10.5 °C at 35 mol% additive ratio as a result of the maximized supercooling induced by the polar *cis*-Azo dopants with steric bulk. Upon further increasing the additive ratio, the incomplete UV charging of *trans*-Azo and the remaining nucleation seeds reduce the degree of supercooling.[15] Non-polar C_{28} alkane shows a similar plot with max. ΔT_C of 3.5 °C at higher (50–60 mol%) additive ratios.

These offset plots for two dissimilar PCM systems show overlapping features when ΔT_C is plotted as a function of mass (as opposed to mol) % of dopants in the composite (Fig. 2b). For both composites, the max. ΔT_C is found at around 50 wt%,
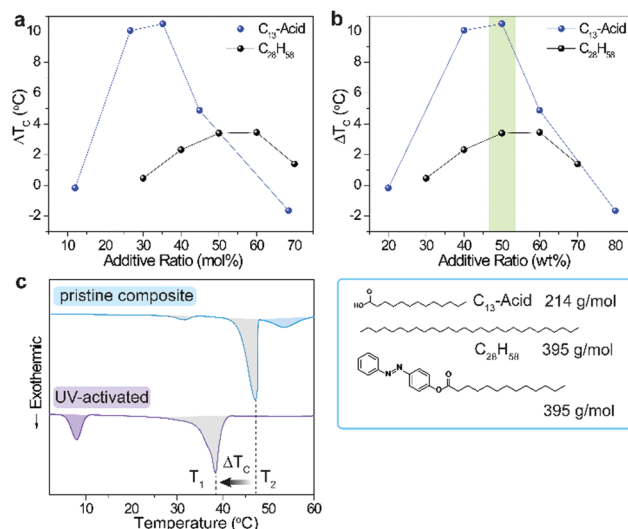
Fig. 2 (a) ΔT_C measured for both C_{13}-acid and $C_{28}H_{58}$ composites while varying the molar additive ratio in composite. (b) ΔT_C plotted against the additive mass ratio in each composite. (c) Differential scanning calorimetry plot of composite (C_{15}-acid with 50 wt% dopants) before and after UV activation. The grey-shaded exothermic peaks represent the crystallization of PCM molecules, and the lowered crystallization point (from T_2 to T_1) is shown. The blue-shaded peak exhibits the crystallization of *trans*-Azo, while the purple-shaded peak shows the crystallization of *cis*-Azo within the composite.

which infers that mass or volume ratio of dopants determines max. ΔT_C independent of the type of PCM. The molecular weight of $C_{28}H_{28}$ is identical to that of the azobenzene dopant, while the molecular mass of C_{13}-acid is about half (54%) that of the azobenzene dopant. Therefore, the degree of supercooling caused by each dopant isomerization in the C_{13}-acid is much higher than in the $C_{28}H_{28}$ as shown in Fig. 2a. Upon identifying the optimal additive ratio (50 wt%), we applied the identical condition to other PCM systems for further investigation and to achieve max. ΔT_C. We also note that the C_{13}-acid composite with the highest additive ratio (80 wt%) has a small negative ΔT_C (-1.7 °C), which is caused by the presence of excess dopant that has a higher T_C (61 °C) than that of the PCM (38 °C). As shown in Fig. S1 (ESI†), both C_{13}-acid and *trans*-Azo are significantly supercooled in the composite even before UV activation, displaying a T_C of 26 °C and 48 °C, respectively. Upon UV irradiation, only 20% *trans-to-cis* isomerization occurs, as analyzed by the integration of differential scanning calorimetry (DSC) exothermic peaks, and the non-uniform dopant mixtures solidify over a broader temperature range of 49–55 °C (Fig. S1, ESI†). In this particular case, ΔT_C is defined as the difference between T_C of excess dopants, which leads to the abnormal and insignificant value.

Fig. 2c shows representative DSC plots taken on a composite (C_{15}-acid, 50 wt% dopant) before and after UV activation. For the uncharged composites, *trans*-Azo solidifies at ~55 °C, followed by crystallization of the PCM at around its intrinsic T_C (T_2). A small exothermic peak ~32 °C represents a minor polymorph of the C_{15}-acid.[24] At any temperature between T_1 and T_2, the heat release from the supercooled liquid PCM composite can be controllably triggered by visible light illumination that isomerizes dopants and creates nucleation seeds of *trans*-Azo.

Fig. 3a shows the average ΔT_C measured for each composite containing 50 wt% photo-switches. Notably, ΔT_C generally decreases as the PCM possesses longer chains and higher melting points (Fig. 3b), except for $C_{15}H_{32}$ which showed a negligible ΔT_C. T_m of the PCM defines the heat storage temperature, and the lower ΔT_C measured at operation temperatures above 50 °C can be explained by the presence of an activation energy for azobenzene reverse isomerization (Fig. 3c). The activation energy for azobenzene derivatives that are mono-functionalized with ester or amide groups is known to be $\Delta H^{\ddagger}$ of 88–92 kJ mol^{-1} and $\Delta S^{\ddagger}$ of -41 to 56 J mol^{-1},[25,26] and the thermal triggering of *cis-to-trans* isomerization occurs at a temperature range of 70–120 °C (Fig. S2, ESI†) in the solid state, which effectively deactivates the photo-switch. Therefore, at higher temperatures, the ratio of *cis* isomer decreases, leaving the discharged *trans*-Azo acting as nucleation seeds in the composite, which in turn results in a lower value for ΔT_C. Once the temperature is as high as 70 °C, there is a very low number of *cis*-Azo molecules in the system, making the difference between the composite before and after UV activation negligible. $C_{15}H_{32}$, despite the low T_m of ~10 °C, showed negligible supercooling, due to the poor miscibility of azobenzene in the short non-polar linear alkane.
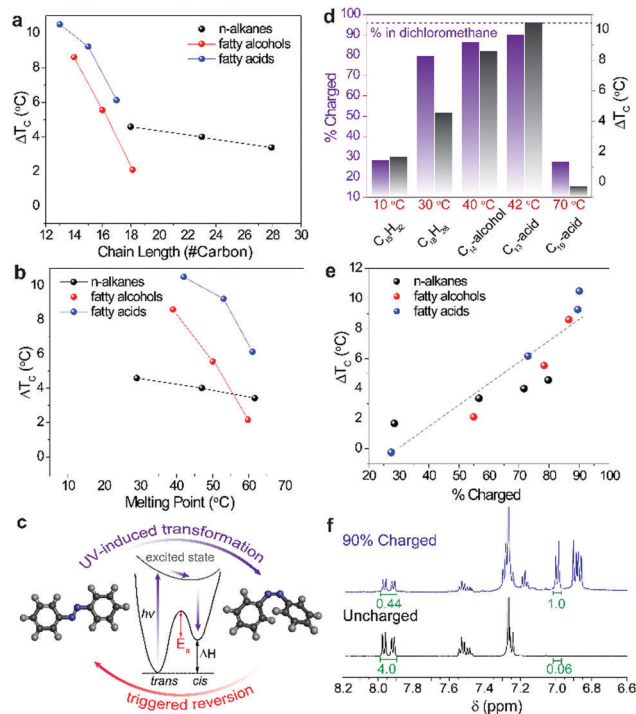

Fig. 3 (a) ΔT_C measured for each composite and plotted against the chain length of each PCM. Composites with comparable charging levels (over 55%) were selected for plotting. (b) ΔT_C plotted against the melting point of each PCM. (c) Energy diagram of azobenzene isomerization highlighting the activation barrier for the triggered reversion process. (d) Charging amount of azobenzene in PCMs measured by ^{1}H NMR and the corresponding ΔT_C value. The purple dotted line represents the max. charging amount of azobenzene dopant in dilute dichloromethane solution (*ca.* 5×10^{-4} M) at 25 °C which allows for unhindered and complete charging due to the low concentration and viscosity of environment, as opposed to that in PCM melt. Depending on the temperature of PCM and miscibility of azobenzene in PCM, the charging amount varies. (e) ΔT_C plotted against charging amount. The dotted line gives visual guidance, showing the correlation between the two terms. (f) Representative ^{1}H NMR plots of PCM composites before (bottom) and after (top) UV activation.

The ratio between *cis* and *trans* isomers after UV activation in each composite can be studied by analysing ^{1}H NMR of the composite, following the UV charging for an identical time period (Fig. 3d). The percent charged indicates the yield of UV-activated *trans-to-cis* conversion. The max charging achieved in dilute solutions (*e.g.* dichloromethane) was 96%, shown for comparison in the figure (dotted line). The bar graphs illustrate the degree of dopant charging in selected composites of varying PCMs where the liquid PCM molecules solvate dopants. The charging amount ranges from 28% to 90% depending on the heat storage temperature as indicated under each graph. We observed that ΔT_C of each composite generally scales with the charging amount which is separately measured by ^{1}H NMR. Fig. 3e confirms that charging amount is indeed one of the most significant factors that influence the degree of supercooling, ΔT_C. In the case of $C_{18}H_{38}$, the charging was very efficient, achieving 80% conversion of azobenzene dopants from *trans* to *cis*, while ΔT_C is lower than the predicted value according to the general trend shown in Fig. 3e. We observed that non-polar PCMs are generally less
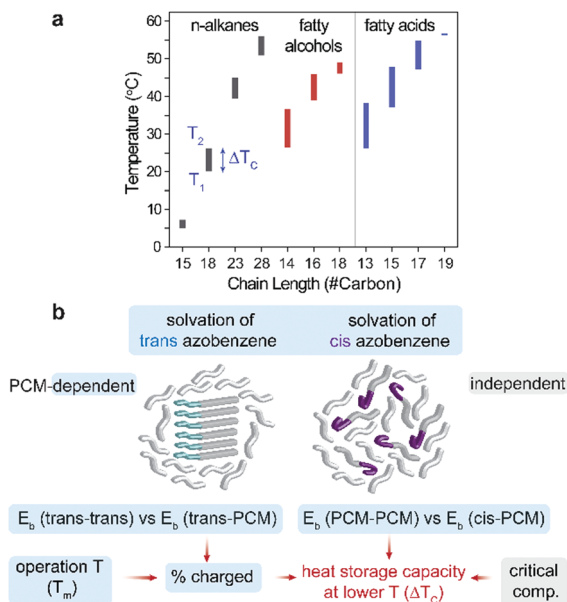
Fig. 4 (a) Summary of key metrics (ΔT_C, T_1, and T_2) of optically-regulated heat storage systems based on various organic PCMs. (b) A schematic illustration describing each PCM-dependent and PCM-independent factor (blue and grey boxed term) that influences ΔT_C. $E_b(\alpha-\beta)$ indicates the binding energy between α and β. T_m is the melting point of the PCM, and the red arrows show the direction of influence.

supercooled than polar counterparts, as a result of the weaker interaction with *cis*-Azo (Fig. S3, ESI†). The measurement of charging amount is performed by integrating the relative ^{1}H NMR peaks that correspond to the aromatic protons on *trans* and *cis* dopants, as shown in Fig. 3f.

Fig. 4a summarizes the measured values, T_1 and T_2, from the charged and uncharged composites containing 50 wt% of azobenzene. This type of chart can provide guidance for the selection of suitable PCM composites for a given application that necessitates a certain condition for heat storage such as storage time. Based on the range of chemistries considered and the comparison between PCM systems with diverse physical properties, we are able to decouple several factors that influence ΔT_C during different stages of the thermal storage cycle (Fig. 4b). Before UV activation, the interaction between molten PCM and *trans*-Azo molecules defines how effectively the additives are solvated by the PCM. If the binding energy (E_b) among *trans*-Azo additives is strong and the solvation is relatively weak, the additives remain aggregated and are less prone to photoswitching upon UV illumination. Therefore, the selection of PCM and its polarity heavily affects the UV charging amount (% charged) which our results show to be one of the most significant factors that determine ΔT_C (Fig. 3e). Once *trans*-Azo is UV activated, the interaction between PCM and *cis*-Azo plays a dominant role in the supercooling process. In this case, if E_b

among PCM molecules is strong relative to E_b between PCM and *cis*-Azo, the crystallization of the PCM is likely to occur as the temperature drops. The selection of a PCM that interacts strongly with the *cis*-Azo can thus enhance stabilization of the liquid PCM composite at lower temperatures, increasing ΔT_C. The operation temperature which is dependent on the PCM selection (Fig. 3b) also determines the charging amount of additives. Lastly, a PCM-independent factor is the critical composition (additive % in the composite), which should be considered when designing the heat storage systems.

Conflicts of interest

There are no conflicts to declare.

Notes and references

1 N. Sarier and E. Onder, *Thermochim. Acta*, 2007, **452**, 149–160.
2 A. M. Khudhair and M. M. Farid, *Energy Convers. Manage.*, 2004, **45**, 263–275.
3 F. L. Tan and C. P. Tso, *Appl. Therm. Eng.*, 2004, **24**, 159–169.
4 E. Oró, A. de Gracia, A. Castell, M. M. Farid and L. F. Cabeza, *Appl. Energy*, 2012, **99**, 513–533.
5 R. K. Sharma, P. Ganesan, V. V. Tyagi, H. S. C. Metselaar and S. C. Sandaran, *Energy Convers. Manage.*, 2015, **95**, 193–228.
6 J. Pereira da Cunha and P. Eames, *Appl. Energy*, 2016, **177**, 227–238.
7 S. A. Memon, *Renewable Sustainable Energy Rev.*, 2014, **31**, 870–906.
8 Y.-J. Jin, B. Shin-Il Kim, W.-E. Lee, C.-L. Lee, H. Kim, K.-H. Song, S.-Y. Jang and G. Kwak, *NPG Asia Mater.*, 2014, **6**, e137.
9 T. Khadiran, M. Z. Hussein, Z. Zainal and R. Rusli, *Sol. Energy Mater. Sol. Cells*, 2015, **143**, 78–98.
10 F. Agyenim, N. Hewitt, P. Eames and M. Smyth, *Renewable Sustainable Energy Rev.*, 2010, **14**, 615–628.
11 K. Kant, A. Shukla, A. Sharma and P. H. Biwole, *J. Energy Storage*, 2018, **15**, 274–282.
12 W. Aftab, X. Huang, W. Wu, Z. Liang, A. Mahmood and R. Zou, *Energy Environ. Sci.*, 2018, **11**, 1392–1424.
13 X. Huang, W. Xia and R. Zou, *J. Mater. Chem. A*, 2014, **2**, 19963–19968.
14 S. Zhang, Q. Tao, Z. Wang and Z. Zhang, *J. Mater. Chem.*, 2012, **22**, 20166–20169.
15 G. G. D. Han, H. Li and J. C. Grossman, *Nat. Commun.*, 2017, **8**, 1446.
16 C. Denekamp and B. L. Feringa, *Adv. Mater.*, 1998, **10**, 1080–1082.
17 T. Ikeda and O. Tsutsumi, *Science*, 1995, **268**, 1873–1875.
18 T. Ikeda, T. Sasaki and K. Ichimura, *Nature*, 1993, **361**, 428–430.
19 A. M. Kolpak and J. C. Grossman, *Nano Lett.*, 2011, **11**, 3156–3162.
20 M. Kenisarin and K. Mahkamov, *Renewable Sustainable Energy Rev.*, 2007, **11**, 1913–1965.
21 T. Kousksou, A. Jamil, T. E. Rhafiki and Y. Zeraouli, *Sol. Energy Mater. Sol. Cells*, 2010, **94**, 2158–2165.
22 Y. Yuan, N. Zhang, W. Tao, X. Cao and Y. He, *Renewable Sustainable Energy Rev.*, 2014, **29**, 482–498.
23 S. Ali Memon, T. Yiu Lo, X. Shi, S. Barbhuiya and H. Cui, *Appl. Therm. Eng.*, 2013, **59**, 336–347.
24 A. D. Bond, *New J. Chem.*, 2004, **28**, 104–114.
25 G. D. Han, S. S. Park, Y. Liu, D. Zhitomirsky, E. Cho, M. Dinca and J. C. Grossman, *J. Mater. Chem. A*, 2016, **4**, 16157–16165.
26 T. J. Kucharski, N. Ferralis, A. M. Kolpak, J. O. Zheng, D. G. Nocera and J. C. Grossman, *Nat. Chem.*, 2014, **6**, 441.